IEEE Access
Multidisciplinary | Rapid Review | Open Access Journal

Received June 24, 2021, accepted August 9, 2021, date of publication August 13, 2021, date of current version August 23, 2021.

Digital Object Identifier 10.1109/ACCESS.2021.3104797

Averaged Dynamic Modeling and Control of a Quasi-Z-Source Inverter for Wind Power Applications

EMANUEL P. P. SOARES-RAMOS[1,2], LAÍS DE OLIVEIRA-ASSÍS[2], RAÚL SARRIAS-MENA[3], PABLO GARCÍA-TRIVIÑO[2], CARLOS ANDRÉS GARCÍA-VÁZQUEZ[2], AND LUIS M. FERNÁNDEZ-RAMÍREZ[2], (Senior Member, IEEE)

[1]Department of Electro-Electronics, Federal Center for Technological Education of Minas Gerais, Curvelo, State of Minas Gerais 35790-000, Brazil
[2]Research Group in Sustainable and Renewable Electrical Technologies (PAIDI-TEP023), Department of Electrical Engineering, University of Cadiz, Cádiz, 11202 Algeciras, Spain
[3]Research Group in Sustainable and Renewable Electrical Technologies (PAIDI-TEP023), Department of Engineering in Automation, Electronics and Computer Architecture and Networks, University of Cadiz, Cádiz, 11202 Algeciras, Spain

Corresponding author: Luis M. Fernández-Ramírez (luis.fernandez@uca.es)

This work was supported in part by the Spain's Ministerio de Ciencia, Innovación y Universidades (MCIU), Agencia Estatal de Investigación (AEI), and Fondo Europeo de Desarrollo Regional (FEDER) Unión Europea (UE) under Grant RTI2018-095720-B-C32, in part by the National Council of Technological and Scientific Development (CNPq), Brazil, in part by the Federal Center for Technological Education of Minas Gerais, Brazil, under Process 23062-010087/2017-51, and in part by the Regional Ministry of Economic Transformation, Industry, Knowledge and Universities of Junta de Andalucía under Grant PY20_00317.

ABSTRACT Typically, permanent magnet synchronous generator (PMSG)-driven wind turbines (WTs) present a two-stage power converter topology based on a DC/DC boost converter and voltage source inverter. In this study, this configuration is substituted by a quasi-Z-source inverter (qZSI), which is an attractive solution for boosting and converting the voltage from DC to AC in a single stage. A 2 MW PMSG WT with qZSI was studied herein. A switched dynamic model (SDM) of the qZSI (including the modeling of all switches and firing pulses) is not recommended for steady-state stability studies, long-term simulations, or large electric power systems. For such studies, two averaged dynamic models are proposed in this work. Both models present the same control system as the SDM, except for the generation of firing pulses, which is not necessary in the averaged models. The two proposed models were evaluated and compared with the SDM in the large-scale WT under different operating conditions, such as wind speed fluctuations, variable power references, and grid disturbances (voltage sag and 3rd and 5th order harmonics injection), in order to demonstrate their adequacy to represent the system response with a high reduction in the simulation time and computational efforts.

INDEX TERMS Control system, modeling, quasi-Z-source inverter, wind turbine.

I. INTRODUCTION

The increase in energy consumption worldwide, associated with growing environmental concerns, poses a challenge to generation systems. For this reason, energy sources based on fossil fuels have been gradually replaced by alternative energy sources. Among the various clean energy sources, wind energy stands out because of the abundance of wind availability. Therefore, the number of high-power wind power plants has increased dramatically.

Among the different variable-speed wind turbine (WT) technologies available, doubly fed inductor generators (DFIGs) and permanent magnet synchronous generators (PMSGs) are usually employed owing to their high energy efficiency [1]–[4]. PMSGs have several advantages, such as high performance, low maintenance compared to DFIGs, and the possibility of direct-drive operation. Detailed information about commercial models of these WTs can be found in [5].

Currently, WTs can have different topologies in terms of their power converters. Some alternatives for the machine-side converter (MSC) of PMSG WTs were suggested in [6], whereas several options for the grid-side converter (GSC)

The associate editor coordinating the review of this manuscript and approving it for publication was Nishant Unnikrishnan.

were presented in [1]. For instance, a three-phase diode bridge can be used as a rectifier for MSCs. However, when the WT rotates at a low speed, the uncontrolled rectifier may not provide the DC voltage level required at the input of the GSC. In these cases, a DC/DC boost converter can be employed to increase the voltage to adequate values for the GSC. This solution is simple, cost-efficient, and allows the extraction of the maximum power from the WT. Nevertheless, it presents high harmonic current distortions in the generator windings, overheating, and oscillations in the torque.

On the other hand, PMSGs can be connected to grid through two two-level voltage source converters (VSCs) in a back-to-back (B2B) configuration and controlled by pulse-width modulation (PWM). Additionally, a voltage transformer is usually inserted between the GSC and the grid. This solution is relatively simple, robust, and reliable. The drawbacks of this configuration are larger switching losses and lower efficiency at high powers, in addition to a high THD [1].

Z-source converters (ZSCs) were proposed in [7] as an improvement to traditional VSCs. ZSCs present a specific structure that achieves a large voltage buck-boost characteristic in a single stage, which is an efficient way to handle power between a source and a load. Single-stage conversion is an attractive option owing to its robustness, reliability, and low cost [7]. In addition, they can work in a shoot-through state without damaging the devices. Several advantages were highlighted in [8], where the configuration based on the DC/DC boost converter and voltage source inverter (VSI) was compared with a configuration based on the ZSC. The ZSC achieved better performance owing to its shoot-through capability. However, its main drawbacks are a discontinuous input current in the boost mode and high-voltage stress in the capacitors of the impedance network [9].

Several ZSC topologies were analyzed in [10]–[13]. The switched trans boost inverter is presented in [10], highlighting its main advantages, such as a high boost factor and a lower number of passive components that reduce size, weight, and cost in comparison with the switched-inductor ZSC. Additionally, a new switched-inductor quasi-Z-source inverter was proposed in [11]. According to the authors, this converter has a continuous input current, a shared DC source ground point, a suppressed startup inrush current, and a high boost voltage inversion ability. Among the different topologies, the quasi-Z-source inverter (qZSI) is particularly attractive owing to several improvements compared to the conventional ZSC [9]. For instance, the qZSI (Figure 1) presents a continuous input current and reduced current and voltage in inductors L_2 and C_2, respectively. Furthermore, it can work as a bidirectional converter by replacing the diode with a bidirectional controlled switch.

Regarding the use of the qZSI with renewable energies, several studies on small-scale photovoltaic solar energy (with rated power below 10 kW) can be found in the literature. The qZSI was used in [14] and [15] for photovoltaic distributed generation with rated powers of 1 kW and 1.3 kW, respectively. In both studies, the closed-loop control of the output voltage/current was applied through the voltage on capacitor C_1 of the impedance network. A model predictive control technique was applied to a 550 W qZSI and PV array system in [16].

Applications based on small-scale wind power generation have also been discussed in the literature. A control strategy for a grid-connected Z-source inverter (ZSI) was presented and compared with a conventional VSI in [17], highlighting the main benefits of the former. A solution using a double-input ZSI was proposed in [18] for a WT with a dual-star PMSG. The authors emphasized the increased generator reliability against short circuits, the need for less passive components, and the desired output voltage waveform as the main advantages.

A dynamic model of the qZSI equipped with an energy storage system was presented in [19], [20]. This converter was used on a PMSG WT in a stand-alone application. Additionally, closed-loop control schemes for the DC and AC sides were presented, validating the adequate performance of the control system through simulation. The authors highlighted the need for further study in this area.

A qZSI can be modeled by a detailed or switched dynamic model (SDM), which includes the modeling of all switches and their firing pulses. However, this model is not recommended for steady-state stability studies, long-term simulations, or large electric power systems because of its large computational requirements. Therefore, a simplified model that can accurately represent the system response while significantly reducing the computational time is an interesting option for such studies. To the best of our knowledge, only the small-signal model described in [21] has been presented as an alternative to the SDM of the qZSI with lower computational efforts. However, it is based on the circuit analysis of the qZSI, rather than on the use of averaged voltage and current sources that can be easily implemented in an electric circuit representation of the qZSI.

In this regard, two averaged dynamic models of the qZSI were developed in this study. These models are implemented using controlled voltage and current sources. The derivation of these models and their control strategies is presented herein. The proposed models can replace the SDM in several scenarios to reduce the simulation time and computational efforts, such as long-term simulations, or large, complex systems with many power sources and/or conversion devices, reproducing a response similar to the SDM. In this work, the averaged models are used for the grid connection of a large-scale WT in a single conversion stage, substituting other traditional configurations that require additional elements. The system was evaluated under different operating conditions. Moreover, the proposed models are compared with the SDM of the qZSI, which includes the individual model of all switches and their firing pulses. The advantages and main characteristics of the averaged models, as well as their limitations, are presented, demonstrating a significant reduction in the simulation time and computational efforts,

making these models a good option for long-term simulation of complex systems.

The main contributions of this paper can be summarized as follows: 1) Derivation of averaged models for the qZSI that can reproduce the performance of a detailed model (with the modeling of all the power switches) with a satisfactory degree of accuracy. By revising the equations of the qZSI, it is possible to express the AC voltage and the DC current in terms of other magnitudes in the system (DC voltage, modulating signal, etc.). This allows substituting the switches in the detailed model for controlled current and voltage sources. This method has already been applied to other power converters in the literature, such as VSC [22] or different DC/DC topologies [23], [24]; however, to the best of our knowledge, it has not been applied to qZSIs. The derivation of such averaged models becomes crucial when performing long-term simulations or simulation of large power systems, given the reduction achieved in the simulation time and computational efforts compared to the detailed model. 2) Evaluation of the performance and control of the averaged models is presented as a part of a large-scale grid-connected wind energy conversion system, where the qZSI substitutes other conventional conversion topologies in such applications.

The paper is organized as follows: Section II presents the configuration of the PMSG WT with qZSI under study. Section III illustrates the modeling and control of switched and averaged dynamic models for qZSI. In Section IV, the simulation results are presented and analyzed. Finally, the most relevant conclusions of this study are presented in Section V.

II. WIND TURBINE WITH qZSI

Figure 1 shows the overall configuration of the PMSG WT with qZSI under study. It uses a full-scale power converter, which is composed of a 3-phase uncontrolled bridge rectifier and qZSI. The use of an uncontrolled rectifier is an economical solution, but it has the main drawback of a significant dependence of the DC bus voltage on the wind speed [6]. Hence, the uncontrolled rectifier usually requires a two-stage power converter based on a DC-DC boost converter and B2B-VSI to control the power flow between the WT and the grid as well as the DC bus voltage. In this work, this two-stage power converter is replaced by a qZSI, which is composed of an impedance network and a 3-phase VSI. The switching control of the VSI allows the regulation of the active power generated by the WT, the reactive power exchanged with the grid, and the DC bus voltage. Finally, an LCL filter is used to reduce the harmonics injected into the grid.

A 2 MW PMSG WT was considered in this study. The rotor of the WT is modeled through the quasi-static model defined by the actuator disk theory, and the drive train is represented by the two-mass model, as is usual in fundamental frequency simulations [25].

The generator is modeled by assuming that the flux distribution in the stator is sinusoidal, by its third-order model, which is defined by the following equations in the synchronous dq reference frame [26].

$$u_{ds} = R_s i_{ds} + L_{ds}\frac{di_{ds}}{d_t} - \omega_e L_{qs} i_{qs} \tag{1}$$

$$u_{qs} = R_s i_{qs} + L_{qs}\frac{di_{qs}}{d_t} + \omega_e \left(L_{ds} i_{ds} + \psi_{pm}\right) \tag{2}$$

$$T_e = \frac{3}{2} p \left(L_{ds} - L_{qs}\right) i_{ds} i_{qs} + \psi_{pm} i_{qs} \tag{3}$$

where u and i denote the voltage and current, respectively; indices d and q are the direct and quadrature components, respectively; index s refers to the stator; R_s and L_s are the stator resistance and inductance, respectively; ω_e is the electrical speed; ψ_{pm} is the permanent magnetic flux; T_e is the electromagnetic torque; and p is the number of pole pairs of the generator.

Each element of the rectifier is modeled as an ideal diode with an RC snubber circuit connected in parallel and a small resistance in series.

A typical qZSI configuration is shown in Figure 1. It consists of a three-level VSI and an impedance network

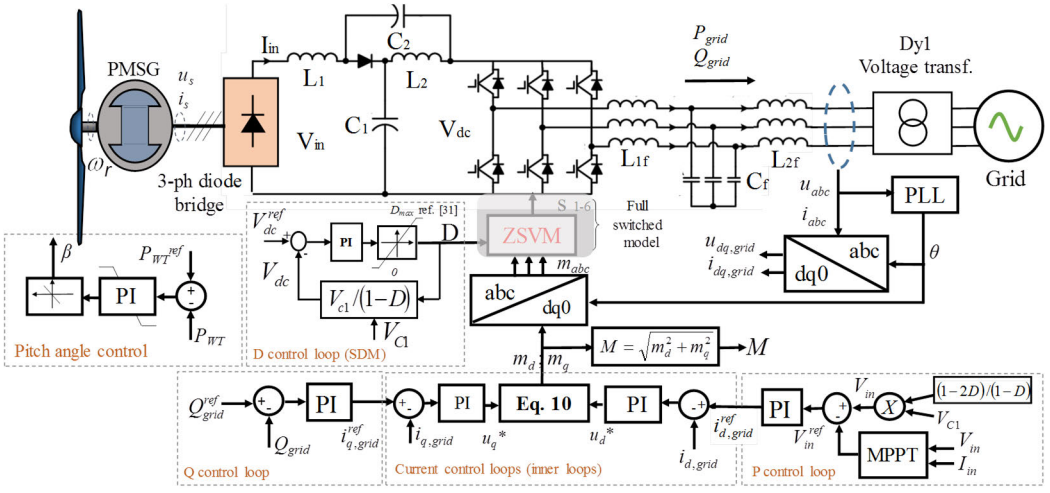

FIGURE 1. General configuration and control of the full switched model of the qZSI.

composed of two capacitors (C_1 and C_2) and two inductors (L_1 and L_2). These components are sized to limit the switching frequency of the current and voltage [27].

The minimum values of the components of the impedance network (L_1, L_2, C_1, and C_2) were calculated according to [28]. Thus, the inductors are sized as follows:

$$L = L_1 = L_2 = \frac{1}{2} T_{0,max} \frac{M_{min} V_{in}}{r_i I_{in}} \tag{4}$$

where r_i is the current ripple (20%), $T_{o,max}$ represents the maximum value of the shoot-through period, M_{min} is the minimum value of the modulation index (M), and V_{in} and I_{in} are the input voltage and current of the impedance network of the qZSI, respectively.

The capacitors are calculated by the following expression:

$$C = C_1 = C_2 = \frac{2T_{o,max} I_{in}(1 - 2D_{max})}{r_v V_{in}} \tag{5}$$

where r_v is the voltage ripple (1%) and D_{max} is the maximum value of the shoot-through duty ratio (D).

In this work, $L_1 = L_2 = 13$ μH and $C_1 = C_2. = 2.5$ mF.

As shown in Figure 1, an LCL filter is considered at the output of the qZSI because it provides high harmonic attenuation and is suitable for large-scale renewable energy applications [29]. Proper sizing of the inductors and capacitors of the filter requires considering the following criteria: 1) the inductor reactance X_{L1} must be lower than 10% of the base impedance to limit the voltage drop; 2) the capacitance C_f is limited to absorb less than 5% of the rated reactive power converter; and 3) to avoid resonance problems, the resonant frequency must remain between ten times the grid frequency and half of the switching frequency [29].

The minimum inductance of L_{1f} can be obtained through [30].

$$L_{1f} = \frac{V_o}{2\sqrt{6} f_s \Delta I_{L1f}} \tag{6}$$

where V_o is the nominal phase-to-ground voltage, f_s is the frequency of the first harmonic of the converter output voltage, and ΔI_{L1f} is the maximum tolerable current ripple.

The minimum capacitance of the filter capacitor (C_f) is calculated by considering the reactive power absorbed by the filter under rated conditions [29].

$$C_f = X_f C_b \tag{7}$$

where X_f is the percentage of the absorbed reactive power (5%), and C_b is the base capacitance.

The minimum inductance of L_{2f} can be determined as a function of L_{1f} [29].

$$L_{2f} = rL_{1f} \tag{8}$$

where r represents the ratio between both inductances.

The values of the filter are $L_{1f} = 0.085$ mH, $L_{2f} = 0.003$ mH and $C_f = 560$ μF.

Finally, a transformer was used to connect the qZSI to the grid. The main parameters of the transformer are as follows: 2.3 MVA, 0.69/33 kV, Dy1, $L_1 = L_2 = 0.001$ p.u., $R_1 = R_2 = 0.03$ p.u., and $R_m = L_m = 500$ p.u, where the base impedance is $Zb = 0.159$ Ω.

III. SWITCHED AND AVERAGED DYNAMIC MODELS OF qZSI

This section describes the SDM of the qZSI, which includes the modeling of all switches and their firing pulses. Then, the two averaged dynamic models (ADMs) for the qZSI are explained, denoted as ADM1 and ADM2, respectively. In these ADMs, the impedance network and the VSI are represented by controlled voltage and current sources, which generate the current and voltage averaged values (AC and DC) over one cycle of the switching frequency. Therefore, these models do not represent the current and voltage harmonics, but they can represent the low-frequency response of the converters in dynamic studies, long-term simulations, and modeling and simulation of large power systems. As a result, the sample time can be increased, resulting in a faster simulation and lower simulation rate. The control schemes for these models, which allow the control of the power exchanged with the grid, are also explained in this section.

A. SWITCHED DYNAMIC MODEL (SDM): DESCRIPTION AND CONTROL

Figure 1 illustrates the SDM of the qZSI, where all the components, including all switches and switching pulses, are modeled.

The control strategy implemented herein is depicted in Figure 1, where the control loops for the active and reactive power, DC bus voltage, and pitch angle can be seen. The aim of the control system is to optimize the power extracted by the wind turbine (P_{WT}) for below-rated wind speeds (maximum power point tracking, MPPT), to limit the power to the rated value of the generator for above-rated wind speeds, to provide the reactive power demanded by the grid and to maintain the DC bus voltage (at the input of the VSI) at its rated value.

To accomplish the aforementioned objectives, a Z-space-vector modulation (ZSVM) technique was applied to the switches of the VSI. Thus, M (index modulation), D (shoot-through duty ratio), and β (pitch angle) are the control variables in the system under study.

In comparison with a traditional SVM technique, where there are six active states and two zero states, the ZSVM applied to the qZSI adds one additional state, called the *shoot-through state*, in which both the upper and lower switches of one or several legs are connected at the same time.

Several ZSVM techniques can be used according to the switching pattern: ZSVM6, ZSVM4, ZSVM2, and ZSVM1. More details about these techniques can be found in [8], [31], [32]. In this work, the ZSVM6 technique is applied owing to two main advantages over other alternatives: a higher voltage gain and a lower voltage stress for the same voltage gain [8].

As in a VSI, in the proposed control scheme, the qZSI is responsible for controlling the active and reactive power

through M. For this reason, a dq reference frame oriented along the grid voltage is used to decouple active and reactive power control. Two cascaded control loops are used to control these powers [22], as shown in Figure 1.

The outer control loops are dedicated to active and reactive power regulation, which can be calculated using Eq. (9) in the dq reference frame. It can be seen that controlling the d and q components of the grid current ($i_{d,grid}$ and $i_{q,grid}$) is equivalent to controlling P_{grid} and Q_{grid}, respectively, because $u_{d,grid}$ is constant in a stiff grid [21].

$$P_{grid} = \frac{3}{2} u_{d,grid} i_{d,grid}$$
$$Q_{grid} = -\frac{3}{2} u_{d,grid} i_{q,grid} \tag{9}$$

The reference values for these currents ($i_{d,grid}^{ref}$ and $i_{q,grid}^{ref}$) are generated by the outer control loops through PI controllers, one controlling active power indirectly through V_{in}, and the other controlling reactive power.

The reactive power reference is imposed externally, whereas the active power depends on the power extracted from the wind. In this sense, an MPPT controller based on the *perturb and observe* algorithm is implemented to define the optimum DC input voltage for the qZSI (V_{in}^{ref}) that achieves maximum power generation in the WT.

The inner loops are the current control loops, where two PI controllers regulate $i_{d,grid}$, and $i_{q,grid}$ to follow the reference values provided by the outer control loops. These PI controllers generate the compensation terms (u_d and u_q). With the contribution of the decoupling terms shown in Eq. (10), independent control of $i_{d,grid}$ and $i_{q,grid}$, and thus, active and reactive power, can be achieved through the d and q components of the modulating signal (namely m_d and m_q) [22].

$$m_d = \frac{2}{V_{DC}} \left(u_d - L_f \omega_0 i_{q,grid} + u_{d,grid} \right)$$
$$m_q = \frac{2}{V_{DC}} \left(u_q - L_f \omega_0 i_{d,grid} + u_{q,grid} \right) \tag{10}$$

where u_d and u_q are the dq components of the qZSI output voltage, L_f is the inductance from the qZSI output to the grid connection ($L_f = L_{1f} + L_{2f}$), and ω_0 is the electric angular frequency.

Once m_d and m_q are determined, they are transformed into m_{abc} (abc/dq transformation) to generate the switching pulses of the qZSI according to the ZSVM6 technique. A phase-locked loop (PLL) ensures tracking of the grid voltage frequency [28]. The magnitude of M can be obtained using m_d and m_q.

Figures 1 and 2a show the control scheme implemented to control D, which is used to maintain V_{dc} around the desired value (1.2 kV). Because measuring V_{dc} is quite difficult and inaccurate in the qZSI, its value is approximated by means of the voltage in C_1 (V_{C1}), as in Eq. (11). A PI controller is used to obtain D from the error between the reference voltage ($V_{dc}{}^{ref}$) and V_{dc}.

$$V_{dc} = V_{C1} \frac{1}{1 - D} \tag{11}$$

The output of the PI controller is limited by the maximum value of D (D_{max}), which is a function of M [31].

Finally, the pitch angle controller of the WT adjusts the blade pitch angle β to reduce the P_{WT}, thus limiting the power generated by the WT for the above-rated wind speeds.

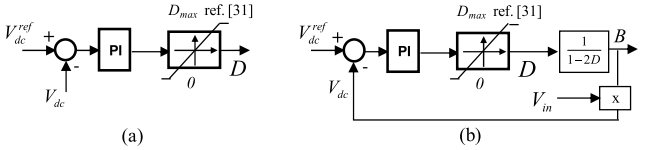

FIGURE 2. V_{dc} control. a) ADM1, and b) ADM2.

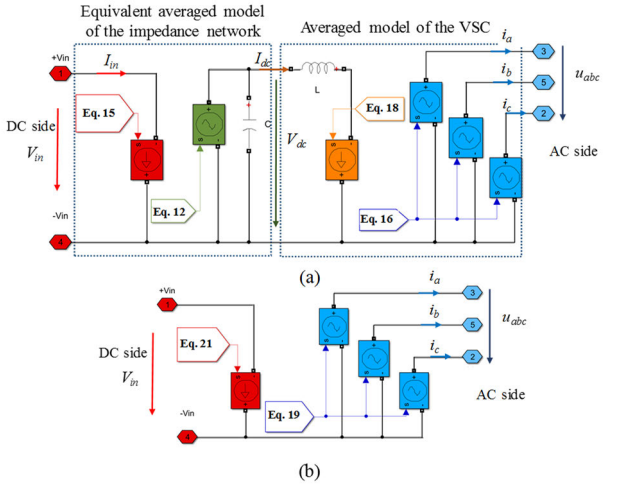

FIGURE 3. Proposed averaged dynamic models (ADMs). a) ADM1 and b) ADM2.

B. AVERAGED DYNAMIC MODEL 1 (ADM1): DESCRIPTION AND CONTROL

In this model, the dynamic response of a qZSI is obtained through the equivalent modeling of two power converters connected in series, one for the impedance network and the other for the VSI, as shown in Figure 3a. This ADM adapts the variable DC input voltage (WT output) to a constant 3-phase AC output voltage. Thus, the voltage boost provided by the impedance network and its behavior are modeled as a conventional DC converter using a switching-function model directly controlled by D [33]. Figures 2a and 2b show the control schemes implemented to control D in ADM1 and ADM2, respectively, which are described in detail in Section III-C.

On the other hand, the VSI is modeled by the averaged equivalent circuit of a three-level VSI, which is composed of a controlled current source at the DC side and three controlled voltage sources at the AC side. In this case, the value of these sources is governed by M, which is output by the control system.

For the equivalent model of the impedance network, the relation between the input (V_{in}) and output (V_{dc}) voltages, assuming a lossless converter, is given by [34]

$$V_{dc} = V_{in} \frac{1}{1 - 2D} \tag{12}$$

The boost factor of the qZSI (B), which represents the voltage gain of the equivalent model, is expressed as follows:

$$B = \frac{1}{1-2D} \tag{13}$$

Therefore, V_{dc} can be calculated from:

$$V_{dc} = V_{in}B \tag{14}$$

It can be derived from a power balance in which the input current (I_{in}) is also related to the output current of the impedance network (I_{dc}) through D.

$$I_{in} = I_{dc}\frac{1}{1-2D} \tag{15}$$

In this model, the output voltage of the VSI u_{abc} is calculated through the modulating signal m_{abc}, which is a balanced 3-phase signal.

$$\begin{aligned} u_a &= \frac{1}{\sqrt{3}}(V_{dc}m_a) \\ u_b &= \frac{1}{\sqrt{3}}(V_{dc}m_b) \\ u_c &= \frac{1}{\sqrt{3}}(V_{dc}m_c) \end{aligned} \tag{16}$$

Assuming a lossless VSI, it implies that the input power on the DC side equals the output power on the AC side.

$$V_{dc}I_{dc} = u_a i_a + u_b i_b + u_c i_c \tag{17}$$

Merging Eqs. (16) and (17), the DC current injected into the VSI can be obtained.

$$I_{dc} = \frac{1}{\sqrt{3}}[i_a m_a + i_b m_b + i_c m_c] \tag{18}$$

The control scheme implemented to generate m_{abc} was the same as that used in the SDM.

C. AVERAGED DYNAMIC MODEL 2 (ADM2): DESCRIPTION AND CONTROL

In ADM2, the dynamic performance of the qZSI is modeled using the averaged model of a VSI. The scheme is composed of a controlled current source at the DC side and three controlled voltage sources at the AC side, as illustrated in Figure 3b.

V_{dc} was not measured, and it was calculated from V_{in} and B (Eq. (14)). Thus, by substituting V_{dc} into Eq. (16), a direct relationship between V_{in} and the AC output voltage can be obtained.

$$\begin{aligned} u_a &= \frac{B}{\sqrt{3}}(V_{in}m_a) \\ u_b &= \frac{B}{\sqrt{3}}(V_{in}m_b) \\ u_c &= \frac{B}{\sqrt{3}}(V_{in}m_c) \end{aligned} \tag{19}$$

Moreover, the following equation can be obtained applying the power balance:

$$V_{in}I_{in} = u_a i_a + u_b i_b + u_c i_c \tag{20}$$

Finally, by substituting Eq. (19) into Eq. (20), the value of I_{in} was calculated.

$$I_{in} = \frac{B}{\sqrt{3}}[i_a m_a + i_b m_b + i_c m_c] \tag{21}$$

Eqs. (19) and (21) show that the input controlled current source and the output controlled voltage source depend on B and m_{abc}, respectively.

In this model, the control schemes for m_{abc} and D are the same as those used in ADM1. A PI controller is used to obtain D from the error between $V_{dc}{}^{ref}$ and V_{dc}, calculated from Eq. (12). D is also limited by D_{max}. Figure 2b illustrates this control scheme for ADM2.

D. STABILITY ANALYSIS OF THE PROPOSED MODELS

The following stability analysis focuses on the DC side of the converter, provided that the AC dynamics rely on the characteristics of the grid connection filter, which is the same for the three models presented. It is well known that the qZSI is an open-loop unstable system with regard to its DC side dynamics [15], [35]. Therefore, a feedback control loop is required to regulate V_{dc}. In this study, a PI controller was implemented in the V_{dc} control loop, as shown in Figure 2. The Bode plot shown in Figure 4 illustrates that both SDM and ADM1 are closed-loop stable systems with such configurations, thus proving the stability of the proposed ADM1.

Regarding ADM2, the DC side dynamics are modeled simply as a static gain that provides the voltage gain of the impedance network in the SDM of the qZSI. Therefore, no stability analysis is required for ADM2.

IV. RESULTS AND DISCUSSION

The system under study (Figure 1) was implemented in MATLAB/Simulink® using the SDM, ADM1, and ADM2 for the qZSI. The main parameters of the PMSG-driven WT model are listed in Table 1.

The time-domain response and control performance of the proposed models were evaluated under different operating conditions: fluctuating wind speed (below and above rated values), variable reactive power reference, and grid disturbances (voltage sag and presence of harmonics in the grid). Three simulation cases were used to test the proposed models, in which the responses of the averaged models (ADM1 and ADM2) were compared with those obtained from the SDM.

A. CASE 1: OPERATION WITH VARIABLE WIND SPEED AND CHANGES IN REACTIVE POWER

Case 1 includes a 80-second simulation with variable wind speed (Figure 5a) between 8.8 (below rated wind speed) and 12.6 m/s (above rated wind speed) and changes in the reactive power reference between -0.2 and 0.2 MVAr (Figure 5c).

As shown in Figure 5b, the active power delivered to the grid is maintained at its rated value for above-rated wind speeds, mainly because of the performance of the pitch angle controller (Figure 5d). For below-rated wind speeds, the pitch angle is kept at 0°, and the WT operates at variable speed

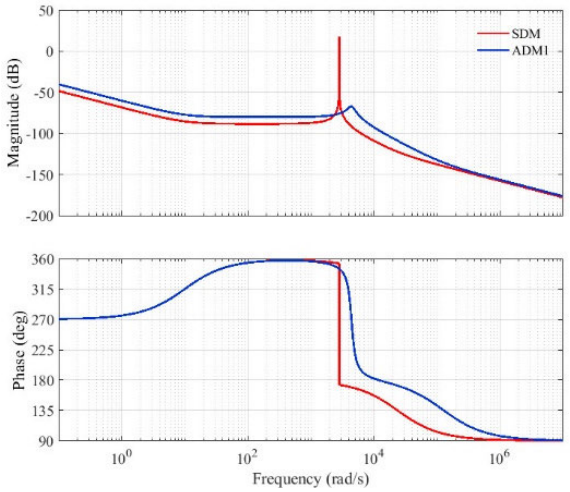

FIGURE 4. Open-loop Bode plot of SDM and ADM1 with controller.

TABLE 1. Parameters of the PMSG.

Parameters	Values
Rated power	2 MW
Grid RMS voltage	0.69 kV
Number of pair of poles	60
Inertia moment	3.1×10^5 kg.m^2
Induced magnetic flux	5.3 Wb
Stator resistance	5.5 mΩ
Stator inductance	0.8 mH
Rated wind speed	11.5 m/s

to inject the maximum power into the grid according to the incoming wind speed. Both ADM1 and ADM2 show similar results to those provided by SDM, with very small differences in pitch angle for above-rated wind speeds and in active power for below-rated wind speeds.

Figure 5c shows the reactive power exchanged with the grid. It can be observed that the WT provides the desired reactive power, which varies between 0.2 and -0.2 MVAr, remaining at zero (unity power factor) for some periods. Regarding the reactive power, the results obtained by ADM1 and ADM2 matched perfectly with those achieved by SDM.

M and D are shown in Fig. 6a. M was used to control the active and reactive powers. It varies significantly with the changes in the reactive power and slightly with the changes in the active power at below-rated wind speeds (variable speed operation). In this case, ADM1 and ADM2 show differences with SDM, although the results obtained for the active and reactive powers are very similar, as illustrated in Figures 5b and 5c.

V_{dc} is perfectly controlled at 1.2 kV (Figure 6b). As shown in Figure 6a, the three models present identical results to control V_{dc} through D.

B. CASE 2: OPERATION WITH GRID DISTURBANCES

The WT and the proposed models are evaluated in Case 2 under two grid disturbances: grid voltage sag and grid voltage with 3rd and 5th harmonics. A 3-second simulation with a constant wind speed of 11.5 m/s (rated wind speed) was performed for both grid disturbances.

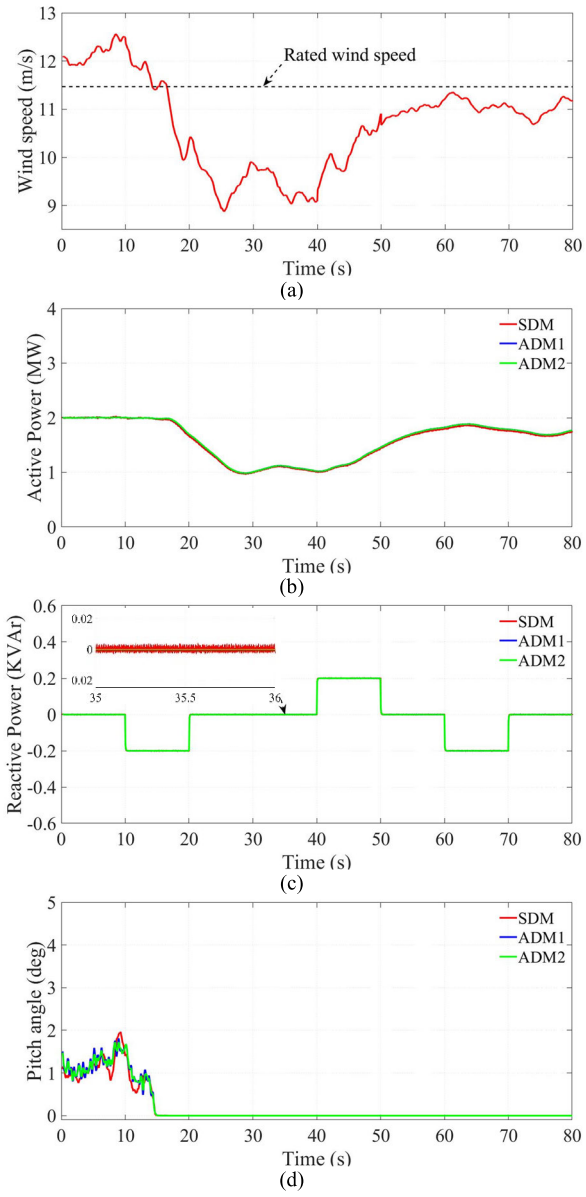

FIGURE 5. Case 1. (a) Wind speed; (b) grid active power; (c) grid reactive power; and (d) pitch angle.

Figure 7 shows the grid voltage and current. Disturbances occur at the second 1. In the simulation with the voltage sag, the grid voltage decreases from 1 to 0.3 pu during 60 ms, whereas in the simulation with harmonics, the 3rd and 5th harmonics in the voltage with an amplitude of 0.08 p.u. each, for 100 ms, are considered. As can be observed, ADM1 and ADM2 can accurately reproduce the grid voltage and current before and after the disturbances.

The active and reactive powers delivered to the grid are shown in Figure 8. As shown, the WT operates at the rated active power and unity power factor before the grid disturbances. During the voltage sag, the active power falls equally in all three models owing to the voltage drop. When the disturbance disappears and the grid voltage is recovered, the active power increases above the rated value transitorily, reaching

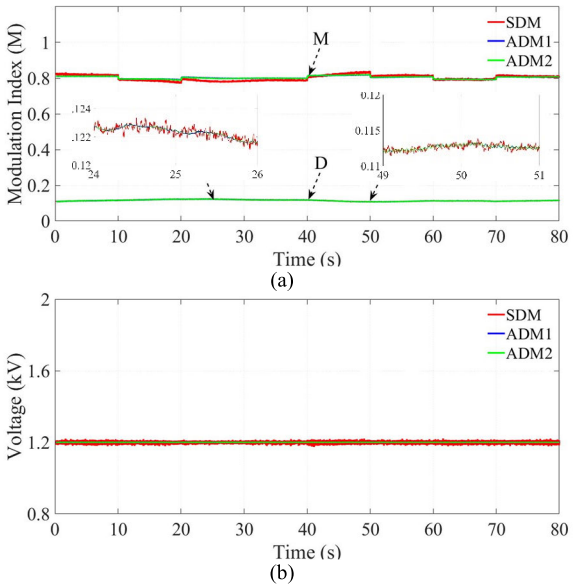

FIGURE 6. Case 1: a) Modulation index (*M*) and Duty cycle (*D*); and b) V_{dc}.

the same maximum value in all three models. Then, owing to the action of the controllers (active power, V_{dc}, and pitch angle controllers), a transient occurs until the steady-state value of the active power (rated active power) is recovered. Some differences between the models were observed in this transient. ADM1 and ADM2 present less variability in the transient and reach pre-fault conditions earlier than SDM. On the other hand, a small variation in the active power can be seen when the other disturbance (grid voltage with 3rd and 5th harmonics) occurs. In both disturbances, the reactive power hardly deviates from zero.

In the case of the voltage sag, ADM1 and ADM2 present less variability in the control variables M and D (Figure 9) than SDM, which explains the differences observed mainly in the active power (Figure 8a) and V_{dc} (Figure 10a). On the contrary, M and D are very little affected by the other grid perturbations, as seen in Figures 9b, 9d, and 10b.

Figure 10 illustrates the control of V_{dc}. In the transient after the voltage sag, significant differences appear for ADM1 and ADM2 compared to SDM because of the simplifications made in the averaged models, although an adequate regulation of V_{dc} can be observed. Finally, as expected, the harmonics in the grid voltage do not affect the control of V_{dc}.

The results obtained show the satisfactory response of the averaged models proposed in this work to represent the steady-state response and control performance of the system under study, although some differences can be observed during the transient response, as expected.

C. COMPUTATIONAL EFFORT

Finally, the models described in Section III are simulated for different time intervals to compare the reduction in the computational effort for ADM1 and ADM2 against SDM. The models were simulated on a computer with an Intel Core i7-4510U processor at 2.60 GHz and 8 GB RAM. As the

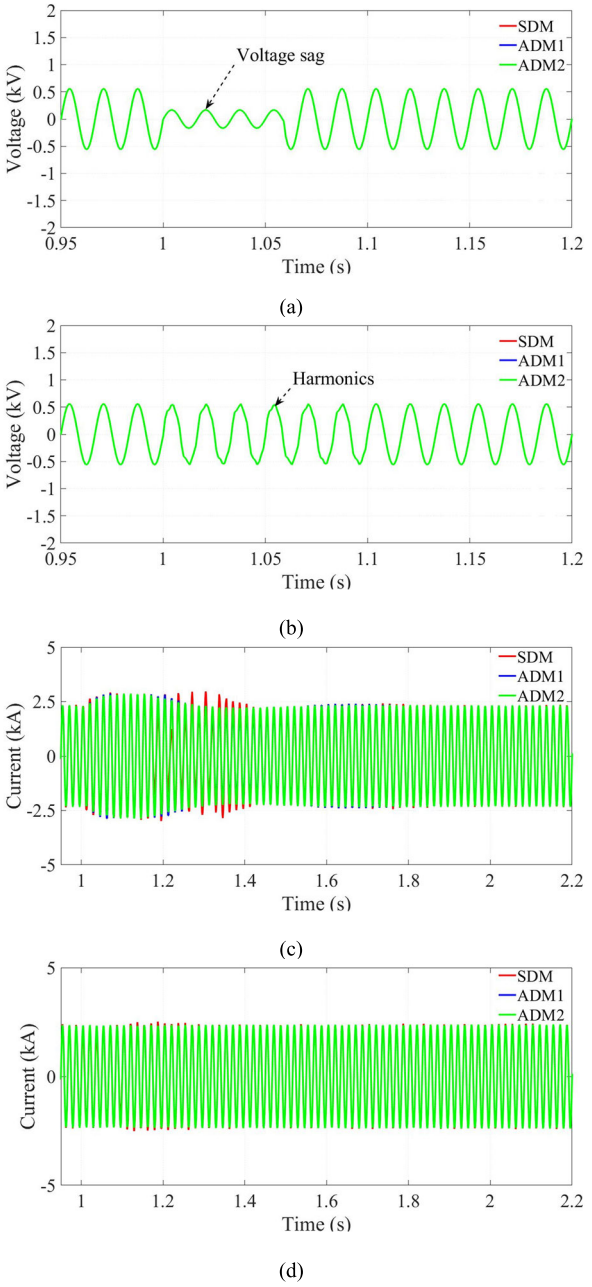

FIGURE 7. Case 2: a) Grid voltage sag: Phase-A voltage; (b) Grid voltage with 3rd and 5th harmonics: Phase-A voltage; (c) Grid voltage sag: Phase-A current; (d) Grid voltage with 3rd and 5th harmonics: Phase-A current.

purpose was to analyze the simulation time and computational effort, the wind turbine was simulated using the rated wind speed and unity power factor.

Table 2 presents the reduction in the simulation time achieved by ADM1 and ADM2 over SDM for several simulation horizons (from 2.5 s to 80 s). Very significant reductions in the simulation time registered for the proposed models compared with the SDM can be observed. ADM1 achieved an average time reduction of 91%, whereas the average reduction was 94% for ADM2. Therefore, ADM2 is the fastest among the models used to represent the time-domain

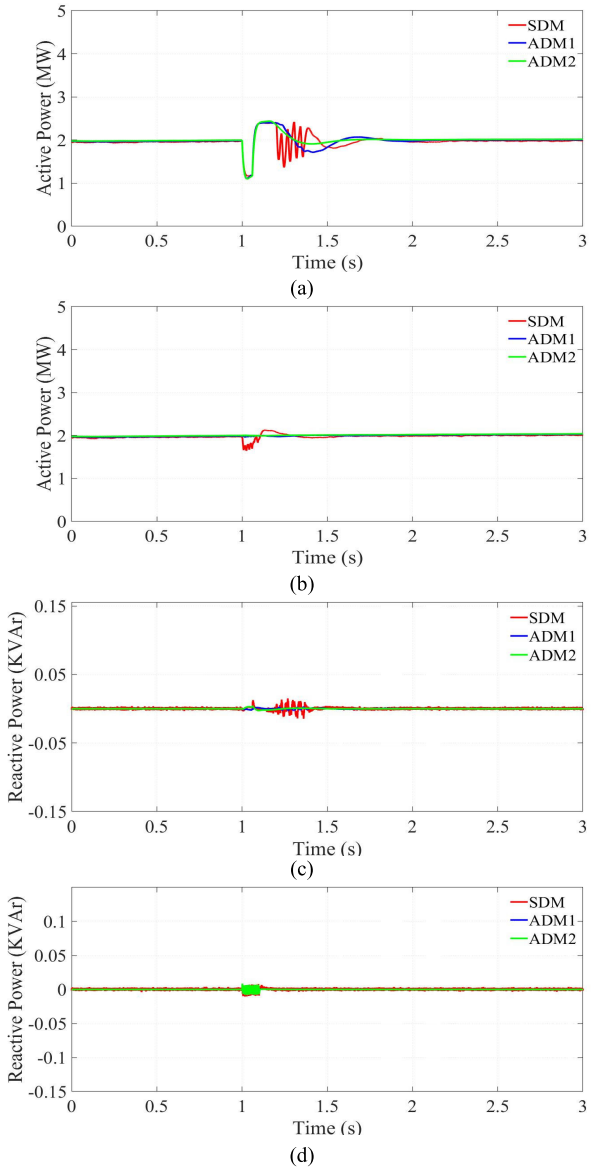

FIGURE 8. Case 2: a) Grid voltage sag: Active power; b) Grid voltage with 3rd and 5th harmonics: Active power; c) Grid voltage sag: Reactive power; d) Grid voltage with 3rd and 5th harmonics: Reactive power.

TABLE 2. Comparison of the computational effort of the models.

	Time reduction (%)		
Simulation horizon (s)	ADM1 vs SDM	ADM2 vs SDM	ADM2 vs ADM1
2.5	83	88	30
5	87	92	37
10	89	94	37
20	92	94	27
30	92	94	24
40	93	95	24
50	94	95	21
60	93	95	25
70	93	95	23
80	94	95	23
Average time reduction	91	94	27

response of the system under study. Furthermore, the average reduction in ADM2 was 27% compared to ADM1.

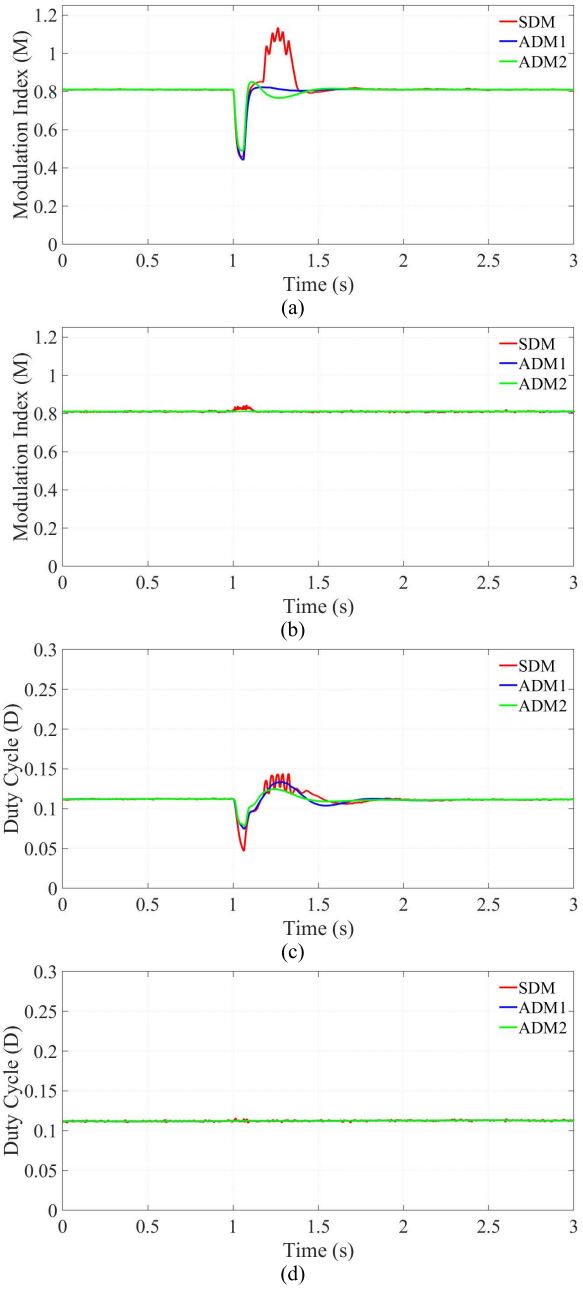

FIGURE 9. Case 2: a) Grid voltage sag: Modulation index (M); b) Grid voltage with 3rd and 5th harmonics: Modulation index (M); c) Grid voltage sag: Duty-cycle; d) Grid voltage with 3rd and 5th harmonics: Duty-cycle.

V. CONCLUSION

Two new averaged models for qZSI were presented in this paper. In ADM1, the voltage boost provided by the impedance network in the qZSI, as well as its dynamic behavior, are modeled as a DC/DC converter using a switching-function model directly controlled through the shoot-through period. This DC equivalent-averaged model of the impedance network is connected to the averaged equivalent circuit of a three-phase VSI. On the other hand, the qZSI is modeled through the averaged model of a VSI with a static gain on the DC side in ADM2, obtaining V_{dc} from V_{in} and boost factor B. Both proposed models are simple, easy

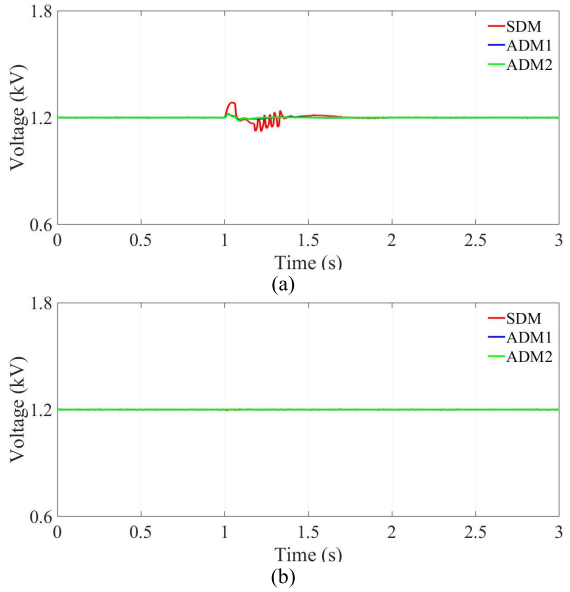

FIGURE 10. Case 2. V_{dc}: a) Grid voltage sag; b) Grid voltage with 3rd and 5th harmonics.

to implement, and to integrate into large power systems as an electric circuit based on controlled voltage and current sources.

These models were used on a 2 MW PMSG-driven WT connected to a grid through an uncontrolled rectifier and a qZSI, where the active and reactive powers delivered to the grid were controlled by the qZSI. The time-domain response and control performances of the proposed models were evaluated under different operating conditions: fluctuating wind speed, variable reactive power reference, and grid disturbances. The results showed a suitable time-domain performance and a significant reduction in the simulation time for both averaged models compared to the SDM (ADM2 reached a 94% reduction in the simulation time). ADM1 showed a better response under grid disturbances than ADM2, which could be expected as ADM2 models the DC dynamics as a static gain. Hence, ADM1 is recommended for studies in which such situations are relevant. ADM2 was 21 times faster than SDM and 1.6 times faster than ADM1 in the best scenario, due to the absence of dynamic states on the DC side. Therefore, ADM2 is preferred, where the speed of simulation and lower computational effort are more valuable than the response to grid disturbances. Notwithstanding the previous remarks, it can be concluded from the results obtained that both proposed averaged models can substitute the SDM with satisfactory accuracy in terms of time-domain response in steady-state stability studies, long-term simulations, or large electric power systems in order to reduce the computational effort and simulation time.

REFERENCES

[1] F. Blaabjerg, M. Liserre, and K. Ma, "Power electronics converters for wind turbine systems," *IEEE Trans. Ind. Appl.*, vol. 48, no. 2, pp. 708–719, Mar./Apr. 2012.

[2] H. H. Aly and M. E. El-Hawary, "An overview of offshore wind electric energy resources," in *Proc. CCECE*, May 2010, pp. 1–8.

[3] Z. Zhang, A. Chen, A. Matveev, R. Nilssen, and A. Nysveen, "High-power generators for offshore wind turbines," *Energy Procedia*, vol. 35, no. 1876, pp. 52–61, 2013.

[4] Z. Zhang, A. Matveev, S. Ovrebo, R. Nilssen, and A. Nysveen, "State of the art in generator technology for offshore wind energy conversion systems," in *Proc. IEEE Int. Electr. Mach. Drives Conf. (IEMDC)*, May 2011, pp. 1131–1136.

[5] I. Arrambide, I. Zubia, and A. Madariaga, "Critical review of offshore wind turbine energy production and site potential assessment," *Electr. Power Syst. Res.*, vol. 167, pp. 39–47, Feb. 2019.

[6] T. R. S. de Freitas, P. J. M. Menegáz, and D. S. L. Simonetti, "Rectifier topologies for permanent magnet synchronous generator on wind energy conversion systems: A review," *Renew. Sustain. Energy Rev.*, vol. 54, pp. 1334–1344, Feb. 2016.

[7] F. Z. Peng, "Z-source inverter," *IEEE Trans. Ind. Appl.*, vol. 39, no. 2, pp. 504–510, Mar./Apr. 2003.

[8] M. Shen, A. Joseph, J. Wang, F. Z. Peng, and D. J. Adams, "Comparison of traditional inverters and Z-source inverter for fuel cell vehicles," *IEEE Trans. Power Electron.*, vol. 22, no. 4, pp. 1453–1463, Jul. 2007.

[9] J. Anderson and F. Z. Peng, "A class of quasi-Z-source inverters," in *Proc. IEEE Ind. Appl. Soc. Annu. Meeting*, Oct. 2008, pp. 1–7.

[10] M. Ghodsi and S. M. Barakati, "A new switched boost inverter using transformer suitable for the microgrid-connected PV with high boost ability," in *Proc. 7th Power Electron. Drive Syst. Technol. Conf. (PEDSTC)*, Feb. 2016, pp. 123–128.

[11] M. Ghodsi, S. M. Barakati, and B. Wu, "Extended switched-inductor quasi-Z-source inverter: Modeling and prototype realization," *Int. Trans. Electr. Energy Syst.*, vol. 29, no. 3, pp. 1–14, 2019.

[12] O. Ellabban and H. Abu-Rub, "An overview for the Z-source converter in motor drive applications," *Renew. Sustain. Energy Rev.*, vol. 61, pp. 537–555, Aug. 2016.

[13] G. Zhang, Z. Li, B. Zhang, and W. A. Halang, "Power electronics converters: Past, present and future," *Renew. Sustain. Energy Rev.*, vol. 81, pp. 2028–2044, May 2018.

[14] Y. Li, F. Z. Peng, J. G. Cintron-Rivera, and S. Jiang, "Controller design for quasi-Z-source inverter in photovoltaic systems," in *Proc. IEEE Energy Convers. Congr. Expo.*, Sep. 2010, pp. 3187–3194.

[15] Y. Li, S. Jiang, J. G. Cintron-Rivera, and F. Z. Peng, "Modeling and control of quasi-Z-source inverter for distributed generation applications," *IEEE Trans. Ind. Electron.*, vol. 60, no. 4, pp. 1532–1541, Apr. 2013.

[16] M. Mosa, H. Abu-Rub, and J. Rodriguez, "High performance predictive control applied to three phase grid connected quasi-Z-source inverter," in *Proc. 39th Annu. Conf. IEEE Ind. Electron. Soc. (IECON)*, Nov. 2013, pp. 5812–5817.

[17] S. Zhang, K.-J. Tseng, D. M. Vilathgamuwa, T. D. Nguyen, and X.-Y. Wang, "Design of a robust grid interface system for PMSG-based wind turbine generators," *IEEE Trans. Ind. Electron.*, vol. 58, no. 1, pp. 316–328, Jan. 2011.

[18] A. R. Dehghanzadeh, V. Behjat, and M. R. Banaei, "Double input Z-source inverter applicable in dual-star PMSG based wind turbine," *Int. J. Electr. Power Energy Syst.*, vol. 82, pp. 49–57, Nov. 2016.

[19] M. M. Bajestan, H. Madadi, and M. A. Shamsinejad, "Controller design for a wind turbine-based variable speed permanent magnet synchronous generator using quasi-Z-source inverter in stand-alone operation," in *Proc. 10th Int. Power Electron., Drive Syst. Technol. Conf. (PEDSTC)*, Feb. 2019, pp. 558–565.

[20] M. M. Bajestan, H. Madadi, and M. A. Shamsinejad, "Control of a new stand-alone wind turbine-based variable speed permanent magnet synchronous generator using quasi-Z-source inverter," *Electr. Power Syst. Res.*, vol. 177, Dec. 2019, Art. no. 106010.

[21] Y. Liu, H. Abu-Rub, B. Ge, F. Blaabjerg, P. C. Loh, and O. Ellabban, *Impedance Source Power Electronic Converters*. Chichester, U.K.: Wiley, 2016.

[22] A. Yazdani and R. Iravani, *Voltage-Sourced Converters in Power Systems: Modeling, Control, and Applications*. Hoboken, NJ, USA: Wiley, 2010.

[23] M. Evzelman and S. Ben-Yaakov, "Simulation of hybrid converters by average models," *IEEE Trans. Ind. Appl.*, vol. 50, no. 2, pp. 1106–1113, Mar. 2014.

[24] T. Pavlovic, T. Bjazic, and Z. Ban, "Simplified averaged models of DC–DC power converters suitable for controller design and microgrid simulation," *IEEE Trans. Power Electron.*, vol. 28, no. 7, pp. 3266–3275, Jul. 2013.

[25] S. Heier, *Grid Integration of Wind Energy: Onshore and Offshore Conversion Systems*, 3rd ed. Hoboken, NJ, USA: Wiley, 2014.
[26] A. Rolan, A. Luna, G. Vazquez, D. Aguilar, and G. Azevedo, "Modeling of a variable speed wind turbine with a permanent magnet synchronous generator," in *Proc. IEEE Int. Symp. Ind. Electron.*, vol. 7, Jul. 2009, pp. 734–739.
[27] L. de Oliveira-Assis, E. P. P. Soares-Ramos, R. Sarrias-Mena, P. Garcia-Trivino, and L. M. Fernandez-Ramirez, "Large-scale grid connected quasi-Z-source inverter-based PV power plant," in *Proc. IEEE Int. Conf. Environ. Electr. Eng. IEEE Ind. Commercial Power Syst. Eur. (EEEIC/I CPS Eur.)*, Jun. 2020, pp. 1–6.
[28] Y. Liu, H. Abu-Rub, B. Ge, F. Blaabjerg, O. Ellabban, and P. C. Loh, *Impedance Source Power Electronic Converters*. Hoboken, NJ, USA: Wiley, 2016.
[29] M. Liserre, F. Blaabjerg, and S. Hansen, "Design and control of an LCL-filter-based three-phase active rectifier," *IEEE Trans. Ind. Appl.*, vol. 41, no. 5, pp. 1281–1291, Sep./Oct. 2005.
[30] D. Krug, M. Malinowski, and S. Bernet, "Design and comparison of medium voltage multi-level converters for industry applications," in *Proc. Conf. Rec. IEEE Ind. Appl. Conf., 39th IAS Annu. Meeting*, vol. 2, Oct. 2004, pp. 781–790.
[31] Y. Liu, B. Ge, H. Abu-Rub, and F. Z. Peng, "Overview of space vector modulations for three-phase Z-source/quasi-Z-source inverters," *IEEE Trans. Power Electron.*, vol. 29, no. 4, pp. 2098–2108, Apr. 2014.
[32] B. Ge, Q. Lei, W. Qian, and F. Z. Peng, "A family of Z-source matrix converters," *IEEE Trans. Ind. Electron.*, vol. 59, no. 1, pp. 35–46, Jan. 2012.
[33] M. K. Kazimierczuk, *Pulse-Width Modulated DC-DC Power Converters*. Hoboken, NJ, USA: Wiley, 2015.
[34] Y. Li, J. Anderson, F. Z. Peng, and D. Liu, "Quasi-Z-source inverter for photovoltaic power generation systems," in *Proc. 24th Annu. IEEE Appl. Power Electron. Conf. Expo.*, Feb. 2009, pp. 918–924.
[35] N. Singh and S. K. Jain, "A novel strategy for indirect control of peak DC-link voltage of grid-connected qZS inverter fed through renewable energy sources," *Electr. Eng.*, vol. 102, no. 2, pp. 611–625, Jun. 2020.

EMANUEL P. P. SOARES-RAMOS was born in Belo Horizonte, State of Minas Gerais, Brazil, in 1987. He received the degree in electrical engineering, in 2012, and the M.Sc. degree in electrical power systems from the Federal Center for Technological Education of Minas Geraisand, in 2014. He is currently pursuing the Ph.D. degree in energy and sustainable engineering with the University of Cadiz, Spain. He is currently a Professor at the Engineering Department of Electro-Electronics, Federal Center for Technological Education of Minas Gerais. He has experience in the area of electrical engineering, working mainly on the following topics: renewable hybrid systems, protection of electrical systems, and electrical machines.

LAÍS DE OLIVEIRA-ASSÍS was born in Belo Horizonte, State of Minas Gerais, Brazil, in 1993. She received the B.S. degree in energy engineering from the Pontificia Universidade Catolica de Minas Gerais, Brazil, in 2017, with partial completion of an undergraduate program at Arizona State University, USA, and the M.S. degree in renewable energy and energy efficiency, in 2018. She is currently pursuing the Ph.D. degree in energy and sustainable engineering with the University of Cadiz, Spain. Her research interests include renewable energy and energy storage systems.

RAÚL SARRIAS-MENA was born in La Línea de la Concepción, Cádiz, Spain, in 1985. He received the M.Sc. degree in industrial engineering and the Ph.D. degree from the University of Cadiz, in 2010 and 2016, respectively.

He is currently an Assistant Professor at the Department of Engineering in Automation, Electronics, and Computer Architecture and Networks, University of Cadiz. His research interests include regulation and control systems for hybrid renewable energy systems and energy storage systems.

PABLO GARCÍA-TRIVIÑO was born in La Línea de la Concepción, Cádiz, Spain, in 1984. He received the B.Sc. degree in electrical engineering, the M.Sc. degree in industrial engineering, and the Ph.D. degree from the University of Cadiz, Cádiz, in 2005, 2007, and 2010, respectively.

Since 2008, he has been an Associate Professor with the Department of Electrical Engineering, University of Cadiz. His research interests include power systems and power management in hybrid systems.

CARLOS ANDRÉS GARCÍA-VÁZQUEZ was born in La Línea de la Concepción, Spain. He received the M.Sc. degree in industrial engineering and the Ph.D. degree from the University of Cadiz, in 2004 and 2009, respectively.

Since 1988, he has been with the Department of Electrical Engineering, University of Cadiz, Algeciras, Spain, where he is currently an Associate Professor. His research interests include electric machines, renewable energy, and smart grids.

LUIS M. FERNÁNDEZ-RAMÍREZ (Senior Member, IEEE) was born in Los Barrios, Cádiz, Spain. He received the M.Sc. degree in electrical engineering from the University of Seville, Seville, Spain, in 1997, and the Ph.D. degree from the University of Cadiz, Cádiz, in 2004.

From 1997 to 2000, he was with the Department of Development and Research, Desarrollos Eolicos S.A., Seville. In 2000, he joined the University of Cadiz, where he is currently an Associate Professor with the Department of Electrical Engineering and the Head of the Research Group in Sustainable and Renewable Electrical Technologies (PAIDI-TEP023). His research interests include smart grids, renewable energy, energy storage, hydrogen systems, electric vehicles, power converters, and control.